

Article

Zircon U-Pb-Hf Isotopes and Whole-Rock Geochemistry of the “Kulumudi Formation” from the Laofengkou Area (West Junggar): Implications of the Construction of a Juvenile Arc in the Junggar–Balkhash Ocean

Bo Liu ^{1,2}, Lin-Xiao Hou ¹, Yan Xu ³, Nan Ju ^{4,5,*}, Jing-Xuan Ma ¹, Zhi-Hao Xie ¹ and Yang-Bai-He Hong ⁶

- ¹ Key Laboratory of Ministry of Education on Safe Mining of Deep Metal Mines, Department of Geology, School of Resources and Civil Engineering, Northeastern University, Shenyang 110819, China; liubo@mail.neu.edu.cn (B.L.); 502023290037@smail.nju.edu.cn (L.-X.H.); 2201068@stu.neu.edu.cn (J.-X.M.)
- ² State Key Laboratory of Continental Dynamics, Northwest University, Xi'an 710069, China
- ³ Ministry of Education, Key Laboratory of Orogenic Belts and Crustal Evolution, School of Earth and Space Sciences, Peking University, Beijing 100871, China; yan_xu@pku.edu.cn
- ⁴ Shenyang Center of China Geological Survey, Shenyang 110034, China
- ⁵ Northeast Geological S&T Innovation Center of China Geological Survey, Shenyang 110034, China
- ⁶ Department of Geological Sciences, Stockholm University, 10691 Stockholm, Sweden; yangbaihe.hong@geo.su.se
- * Correspondence: junan@mail.cgs.gov.cn

Abstract: The properties of ancient magmatic arcs are crucial for understanding the tectonic evolution of the Central Asian Orogenic Belt. The Middle Devonian Kulumudi Formation in the Laofengkou area of West Junggar lacks accurate chronological data constraints, which hampers the knowledge of the nature of the Late Paleozoic magmatic arcs in the West Junggar and circum-Balkhash areas. In this contribution, samples of pyroclastic rocks and sedimentary rocks were collected from the volcano–sedimentary strata of the Kulumudi Formation. Petrography, zircon U-Pb-Hf isotopic analysis and whole-rock geochemistry were carried out to constrain the age and the tectonic setting of the Kulumudi Formation. The zircon U-Pb age of the lithic crystal tuff from the Kulumudi Formation on the northeast side of the Alemale Mountains was 386 ± 2 Ma, accurately indicating that this rock unit formed during the Middle Devonian. However, the fine sandstone near the Huojierte Mongolian Township, originally assigned as the “Kulumudi Formation”, yielded a maximum depositional age of 341 ± 3 Ma. Combined with the stratigraphic contact, this rock unit was redefined to belong to the Lower Carboniferous Jiangbasitao Formation. According to the whole-rock geochemistry study, the lithic crystal tuff of the Kulumudi Formation was characterized as medium potassium–calc–alkaline series rock, which is relatively enriched in light rare earth elements and large ion lithophile elements (i.e., Rb, Ba, K) and depleted in high-field-strength elements (i.e., Nb, Ta, Ti), showing similar geochemical characteristics to the volcanic arc rocks. By contrast, the fine sandstone from the Jiangbasitao Formation had $\text{Al}_2\text{O}_3/\text{SiO}_2$ (0.25–0.29) and $\text{K}_2\text{O}/\text{Na}_2\text{O}$ (1.29–1.72) ratios close to those derived from the continental arc and active continental margin and was characterized as part of the continental arc field in the La-Th-Sc and Th-Sc-Zr/10 tectonic discrimination diagrams. Zircon Hf isotope analysis showed that the $\epsilon_{\text{Hf}}(t)$ values of the Kulumudi Formation were +5.6–+12.8, and those of the Jiangbasitao Formation were +11.43–+15.48, both of which show highly positive juvenile characteristics. The above data indicate that the Kulumudi Formation and Jiangbasitao Formation both formed in a juvenile arc setting with ocean–continent subduction. Combined with the previous work, it was concluded that the southward subduction of the ocean basin represented by the Darbut–Karamay ophiolitic mélanges beneath the newly accreted arc crustal segments produced a juvenile arc with positive Hf isotope characteristics.

Keywords: Kulumudi Formation; West Junggar; Junggar–Balkhash Ocean; Central Asian Orogenic Belt; Hf isotope



Citation: Liu, B.; Hou, L.-X.; Xu, Y.; Ju, N.; Ma, J.-X.; Xie, Z.-H.; Hong, Y.-B.-H. Zircon U-Pb-Hf Isotopes and Whole-Rock Geochemistry of the “Kulumudi Formation” from the Laofengkou Area (West Junggar): Implications of the Construction of a Juvenile Arc in the Junggar–Balkhash Ocean. *Minerals* **2024**, *14*, 14. <https://doi.org/10.3390/min14010014>

Academic Editor: Jean-Michel Lafon

Received: 24 October 2023
Revised: 11 December 2023
Accepted: 16 December 2023
Published: 21 December 2023



Copyright: © 2023 by the authors. Licensee MDPI, Basel, Switzerland. This article is an open access article distributed under the terms and conditions of the Creative Commons Attribution (CC BY) license (<https://creativecommons.org/licenses/by/4.0/>).

1. Introduction

The Central Asian Orogenic Belt (CAOB), or the Altaiids [1], is located between the Siberian Craton, the European Craton and the Tarim–North China Craton (Figure 1a). It is characterized by the significant accretion of arcs (both intra-oceanic and continental), accretionary complexes, seamounts and oceanic plateaus since the Neoproterozoic, which formed during the long-term evolution of the Paleo-Asian Ocean [2,3]. The CAOB is a complex collage that consists of three major oroclines, including the Kazakhstan Orocline [4], the Mongolian Orocline [5] and the NE China Orocline [6]. Among these, the formation of the Kazakhstan Orocline has been attributed to the large-angle bending of the Devonian–Carboniferous magmatic arcs during the Late Paleozoic consumption of the Junggar–Balkhash Ocean (the southwestern branch of the Paleo-Asian Ocean) [2,4,7–10]. These two Devonian–Carboniferous magmatic arcs are difficult to reconstruct using a traditional study of igneous rocks because of the long-term subduction erosion [11]. However, the arc-derived sedimentary rocks retained on the surface might have recorded information about the provenances [11,12]. By using whole-rock geochemical compositions and detrital zircon U-Pb-Hf isotope characteristics of these arc-related sedimentary rocks, we can trace the properties of ancient magmatic arcs. Moreover, compared with the well-accepted Early-to-Middle-Devonian outer arc belt (OAB) with a Precambrian continental basement, the basement nature of the Late-Devonian-to-Carboniferous inner arc belt (IAB) remains debated [9,10,13].

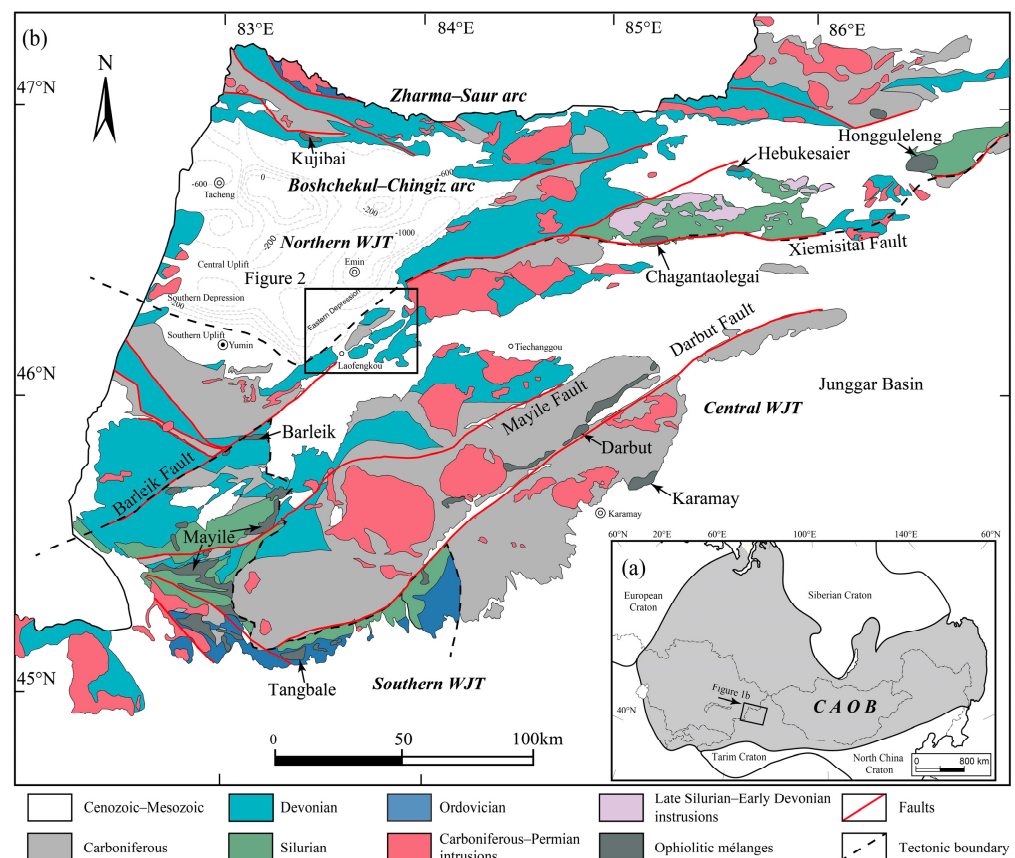


Figure 1. (a) Simplified tectonic map of the Central Asian Orogenic Belt (modified after [14]). (b) Geological map of the West Junggar terrane (modified after [15]).

The West Junggar Terrane (WJT) in the southwestern CAOB is located on the northern limb of the Kazakhstan Orocline (Figure 1a) [9,10]. The WJT is characterized by widespread Paleozoic accretionary complexes and Carboniferous–Permian intrusive rocks (Figure 1b), and its formation was closely associated with the subduction and closure of the Junggar–Balkhash Ocean [2,7,16–18]. Current research on the tectonic evolution of the WJT

focuses on the Ediacaran–Early Paleozoic [15,17,19,20] and Carboniferous–Permian periods [14,18,21]. It is generally accepted that the Ediacaran–Early Paleozoic evolution of the WJT was dominated by a single or multiple intra-oceanic arc(s) [15,17,19,20,22,23]. Previous work showed that the WJT was a place of active convergence during the Early Carboniferous [24,25], while the Late Carboniferous–Permian tectonic setting was suggested to be a post-collisional [25–27] or continuous normal/ridge-related subduction system [7,28,29]. However, relatively little research has been focused on the Devonian tectonic evolution of the WJT [9,30]. Therefore, a timely study of the Devonian tectonic setting is the key to understanding the whole Paleozoic tectonic evolution of the Junggar–Balkhash Ocean.

The Laofengkou area is located in the central part of the WJT, where the Late Paleozoic volcano–sedimentary strata and the Carboniferous–Permian intrusive rocks are extensively outcropping (Figure 2), but the accurate sedimentary age of the Middle Devonian Kulumudi Formation is still unclear. In this contribution, samples of pyroclastic rocks and sedimentary rocks were collected from the Middle Devonian Kulumudi Formation (Figure 2). Petrography, zircon U–Pb–Hf isotopic and whole-rock geochemistry analyses were carried out to accurately constrain the age and tectonic setting of the Middle Devonian Kulumudi Formation, which could provide new insights into the Late Paleozoic evolution of West Junggar. Combined with published data from the West Junggar and circum-Balkhash areas, the nature of the Late Paleozoic magmatic arcs in the tectonic frame of the Kazakhstan Orocline is discussed.

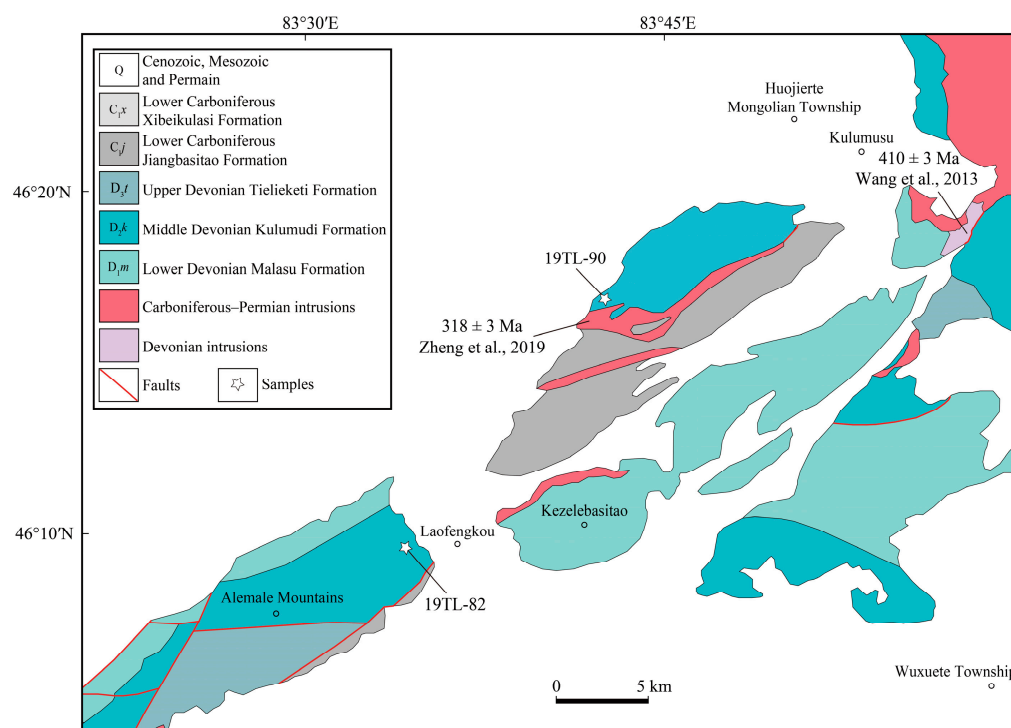


Figure 2. Geological map of the Laofengkou area (modified after [31]). Published age data are from [22,32].

2. Geological Setting and Sampling

2.1. Tectonic Units of the WJT

The WJT is located at the junction of the Siberian and Kazakhstan–Yili plates (Figure 1a), sandwiched between the North Tianshan and the Irtysh–Zaisan suture zones. According to juvenile Sr–Nd–Hf isotopic data, the WJT has been interpreted to lack of ancient Precambrian continental basement [16,33,34]. Taking the Chagantaolegai ophiolite mélangé [35,36] and the Barleik–Mayile–Tangbale ophiolite mélangés as the tectonic boundary (Figure 1b; [21,37]), the WJT can be divided into the northern, central and southern parts.

The northern WJT is composed of the Zharma–Saur arc and Boshchekul–Chingiz arc from north to south, which are separated by the EW-trending Kujibai–Hebukesaier–Hongguleleng ophiolitic mélanges [36,38]. The Zharma–Saur arc (346–321 Ma [24]) formed during the southward subduction of the Irtysh–Zaisan Ocean [2,24,39,40], while the Boshchekul–Chingiz arc is supposed to be related to the northward subduction of the Junggar–Balkhash Ocean [2,41] or the southward subduction of the Irtysh–Zaisan Ocean [42,43] during the Late Silurian–Early Devonian period.

The central WJT is dominated by the Late Paleozoic accretionary complexes (Figure 1b) and Late Carboniferous–Early Permian granitoids [26,27]. Based on the recent identification of Late Devonian diorite (~368 Ma) with typical juvenile Nd isotopes, the central WJT was suggested to be the eastern extension of the northern limb of the IAB [9]. The Devonian–Early Carboniferous Karamay and Darbut ophiolitic mélanges [44–47] occur in the accretionary complexes and represent the youngest ophiolite mélanges in the WJT. The Paleozoic volcano–sedimentary sequences of the central WJT can be divided into the Mayile Mountains area and Karamay area. In the Mayile Mountains area, the Devonian strata are dominated by the Kulumudi and Tielieketi formations, comprising a set of clastic and volcanic rocks under neritic to marine environments [21,31,37,48–50]. The zircon U–Pb ages of the tuffs from the Tielieketi Formation range from ~369 to 363 Ma [21,50], and the maximum depositional age of this formation is ~356 Ma [21]. The Lower Carboniferous strata include the Heishantou and Jiangbasitao formations, and the zircon U–Pb ages of tuffs from the latter are ~336 to 339 Ma [51]. The Paleozoic strata exposed in the Karamay area include the Carboniferous and Permian volcano–sedimentary rocks. The Lower Carboniferous strata consist of the Tailegula, Baogutu and Xibeikulasi formations, and there are different understandings of the stratigraphic sequences among them [52–55]. A limited outcrop of the Upper Carboniferous Molaoba Formation shows typical fluvial sedimentary characteristics [21]. Upwards, Permian volcano–sedimentary sequences are a set of intermediate-acid terrestrial volcanic rocks containing fossils of Angara flora [56,57].

The southern WJT contains the Ediacaran–Silurian arc and accretionary complexes. The records of intra-oceanic arc magmatism are mainly distributed in the Barleik (540–502 Ma [22,37,58]), Mayile (530–515 Ma [20,23]) and Tangbale (572–549 Ma [22,23]) areas. The accretionary complexes are mainly composed of the Barleik, Mayile and Tangbale SSZ-type ophiolite mélanges from north to south and the subduction-related metamorphic rocks (504–492 Ma [17]). Previous studies have found that the oldest ophiolitic mélanges of the southern WJT formed at 572 to 512 Ma [20,59–61], suggesting that the initial intra-oceanic subduction of the Junggar–Balkhash Ocean occurred in the Ediacaran [15]. Recently, the occurrences of quartz diorites with adakitic geochemical features (394–390 Ma [10]) were interpreted as supporting evidence of an eastern extension of the Kazakhstan OAB in the southern WJT.

2.2. Geology of the Study Area

The Laofengkou area is located in the northeast of the Mayile Mountains in the central WJT and is dominated by the Devonian–Early Carboniferous strata and granitoid intrusions (Figure 2). The Middle Devonian Kulumudi Formation is composed of littoral–shallow marine terrigenous sedimentary rocks, pyroclastic rocks with a small amount of limestone and acid volcanic rocks [31]. The zircon U–Pb age of the tuff for the Kulumudi Formation near the Laofengkou area (Tiechanggou area, Figure 1b) is 379 ± 5 Ma [48]. In terms of the Laofengkou area, the Middle Devonian Kulumudi Formation exposed northeast of the Alemale Mountains consists of tuffaceous siltstone and lithic crystal tuff (Figure 3a). Meanwhile, the Kulumudi Formation is composed of fine sandstone interbedded with sandstone southwest of the Huojierte Mongolian Township (Figure 3d).

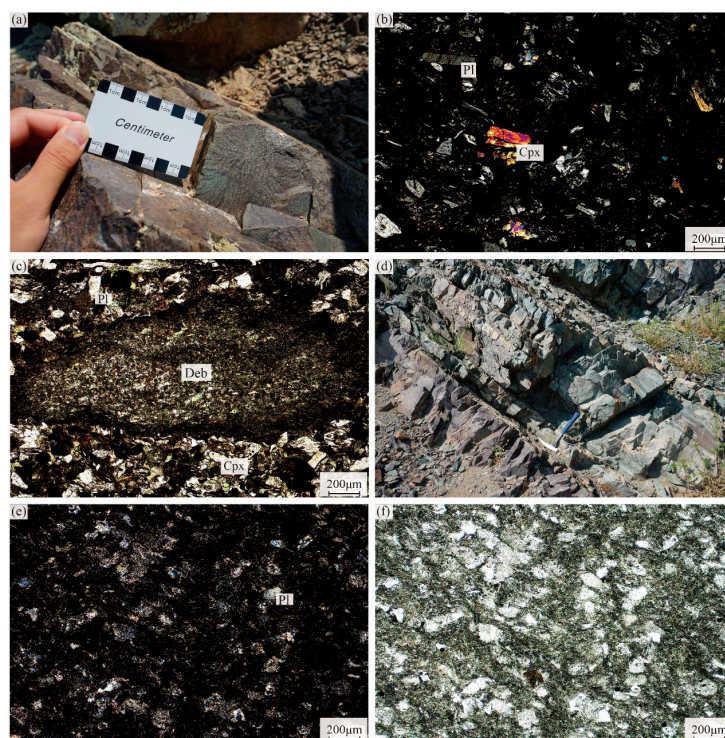


Figure 3. Photomicrographs and field photographs of the dark green lithic crystal tuff (a–c) and gray-green fine sandstone (d–f). Pl—plagioclase; Cpx—clinopyroxene; Deb—debris.

2.3. Sample Description

Samples were collected from the above locations (Figure 2), including the lithic crystal tuff and fine sandstone. The dark green lithic crystal tuff (19TL-82, 46°7′48″ N, 83°35′57″ E) had a tuffaceous texture and massive structure (Figure 3a), which was mainly composed of crystal debris (65%), lithic debris (25%) and volcanic ashes (10%) (Figure 3b,c). The crystal debris consisted of plagioclase (0.2–0.7 mm) and clinopyroxene (~0.2 mm). Locally, this sample had undergone clayization. The gray-green fine sandstone (19TL-90, 46°17′20″ N, 83°42′22″ E) showed a fine-grained texture and massive structure (Figure 3d). It developed plenty of xenomorphic carbonate minerals and a few plagioclases with altered edges and polysynthetic twins (Figure 3e,f).

3. Analytical Methods

3.1. Zircon U–Pb and Lu–Hf Isotope Analysis

Representative zircon grains were selected from the samples according to their color, shape and integrity; mounted in epoxy resin; and polished. The zircon grains with obvious oscillating zoning under cathodoluminescence (CL) images were considered. Zircon U–Pb dating and trace element analyses were undertaken using laser ablation inductively coupled plasma mass spectrometry (LA-ICP-MS) at Beijing Createch Testing Technology Co., Ltd., Beijing, China, using a RESolution 193 nm laser ablation system attached to an Agilent 7500 ICP-MS instrument. The laser spot was 24 μm in diameter, and the frequency was 10 Hz. The energy density was about 10 J/cm². GJ-1 standard zircons were used during the experiments. Offline data calculations and concordia diagrams were processed using the ICPMSDataCal program [62] and Isoplot 4.0, respectively. The zircon U–Pb data and rare earth element compositions are summarized in Table S1 and Table S2, respectively.

In situ zircon Hf isotope analysis was carried out using a RESolution SE 193 laser-ablation system attached to a Nu Plasma II multiple collector ICP-MS instrument at State Key Laboratory of Continental Dynamics, Northwest University, Xi’an, China. Zircon GJ-1 was used as the standard sample. The laser spot was 43 μm in diameter and the energy density was 6 J/cm². The detailed experimental process and related parameters are

described by [63,64]. A two-stage model was selected for the depleted-mantle-based Hf model ages (T_{DM}) calculation. The zircon Hf data are summarized in Table S3.

3.2. Whole-Rock Major and Trace Element Analysis

The whole-rock major and trace element compositions were determined at Beijing Createch Testing Technology Co., Ltd., Beijing, China. Major elements were analyzed using a Shimadzu X-ray fluorescence spectrometer with an accuracy better than 5%. The trace elements were determined using an Analyticjena PQMS elite ICP-MS with an accuracy better than 5%. The analytical data are presented in Table S4.

4. Analytical Results

4.1. Zircon U-Pb and Lu-Hf Isotope Analysis

4.1.1. Zircon U-Pb Ages

Zircons from the lithic crystal tuff (19TL-82) were mainly euhedral and prismatic with lengths of 50–150 μm and showed obvious oscillatory zoning (Figure 4a), which is typical of tuff origin [65]. Based on REE patterns (Table S2), zircons shown by the solid lines exhibited positive Ce and slightly negative Eu anomalies, which is typical of igneous origin (Figure 5a). This is consistent with their Th/U ratios (0.31–0.97, Table S1). Zircons shown by the dotted line were relatively rich in La (Figure 5a), which might have been subjected to hydrothermal metasomatism or metamorphism at a later stage [66], and were excluded from consideration. This sample yielded 30 valid zircon ages ranging from 380 ± 4 Ma to 421 ± 7 Ma ($^{206}\text{Pb}/^{238}\text{U}$ age, Table S1), of which the older age of 421 ± 7 Ma might have been derived from an inherited zircon. The weighted mean $^{206}\text{Pb}/^{238}\text{U}$ age of the remaining 29 zircons was 386 ± 2 Ma (MSWD = 1.20, Figure 6a,b), representing that the lithic crystal tuff formed during the Middle Devonian.

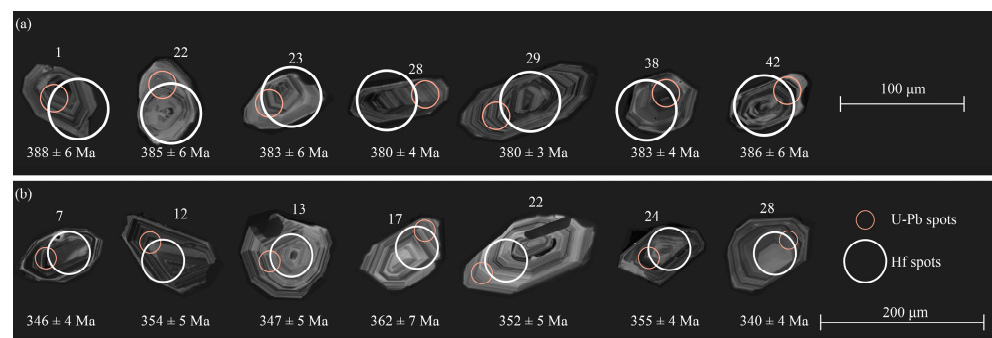


Figure 4. Cathodoluminescence (CL) images of representative zircons of the lithic crystal tuff (a) and fine sandstone (b).

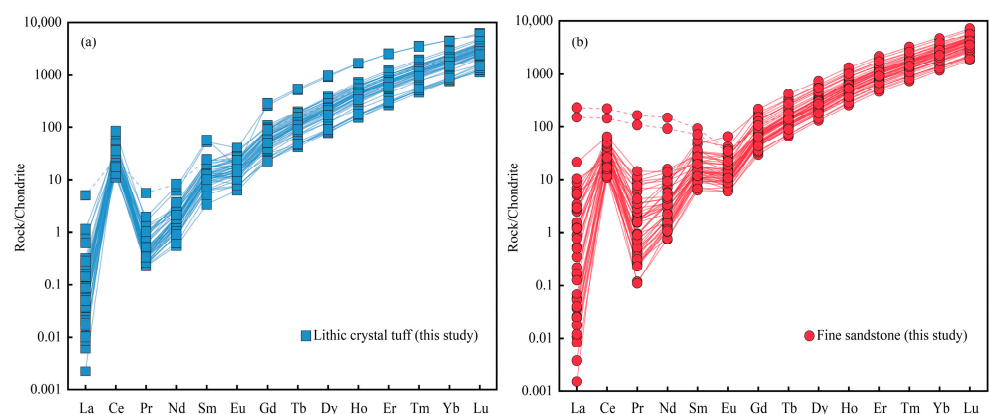


Figure 5. Chondrite-normalized REE patterns of the zircons of the lithic crystal tuff (a) and fine sandstone (b). Chondrite normalization values are from [67].

Detrital zircons from the fine sandstone (19TL-90) were mainly euhedral and short prismatic, with clear oscillating zoning and 50–200 μm in length (Figure 4b). Zircons shown by the dotted lines were also not considered (Figure 5b, Table S2). The sample yielded 48 usable zircon ages with a variation from 340 ± 4 Ma to 382 ± 5 Ma, with Th/U ratios ranging from 0.40 to 1.11 (Table S1). The Early Carboniferous ages comprised the largest population (41 of the 48 results, Table S1) and exhibited a single peak at 350 Ma (Figure 6c,d). The maximum depositional age of this sandstone was 341 ± 3 Ma ($^{206}\text{Pb}/^{238}\text{U}$ age, $n = 5$) using the weighted mean age of the youngest cluster of two or more grain ages ($n \geq 2$) overlapping in age at 1σ (YC1 σ (2+)).

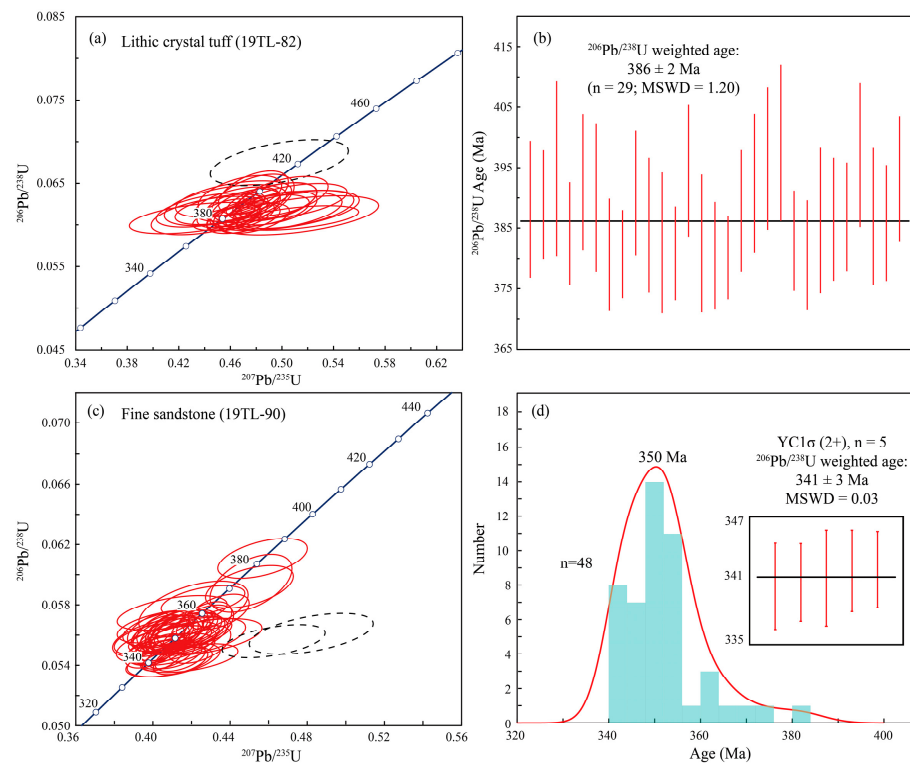


Figure 6. Zircon U-Pb concordia diagrams and weighted average age diagrams of the lithic crystal tuff (a,b) and fine sandstone (c,d). The red solid circles represent valid zircon ages that were used for further discussion, whereas the black dotted ones were not considered during the calculation.

4.1.2. Hf Isotopes

Nineteen zircon grains from the lithic crystal tuff that were selected for U–Pb dating were analyzed for in situ Lu–Hf isotopic compositions. They had initial $^{176}\text{Hf}/^{177}\text{Hf}$ ratios from 0.282685 to 0.282895 (Table S3) and exhibited $\epsilon_{\text{Hf}}(t)$ values from +5.6 to +12.8 (Figure 7a). All zircon grains were characterized by young Hf model ages of 564–1032 Ma (Table S3).

Twenty-eight detrital zircon grains from the fine sandstone had initial $^{176}\text{Hf}/^{177}\text{Hf}$ ratios from 0.282931 to 0.282991 (Table S3) and their $\epsilon_{\text{Hf}}(t)$ values ranged from +11.4 to +15.5, consistent with the Early Carboniferous sedimentary rocks in the adjacent area (Figure 7b). These detrital zircons had comparable young Hf model ages of 366–626 Ma (Table S3).

4.2. Whole-Rock Major and Trace Element Analysis

The whole-rock geochemical analysis was carried out for the lithic crystal tuff (19TL-80/81) and fine sandstone (19TL-88/89). To avoid the influence of loss on ignition (LOI), all contents for major oxides were recalculated after deducting the LOI. Whole-rock geochemical data are shown in Table S4.

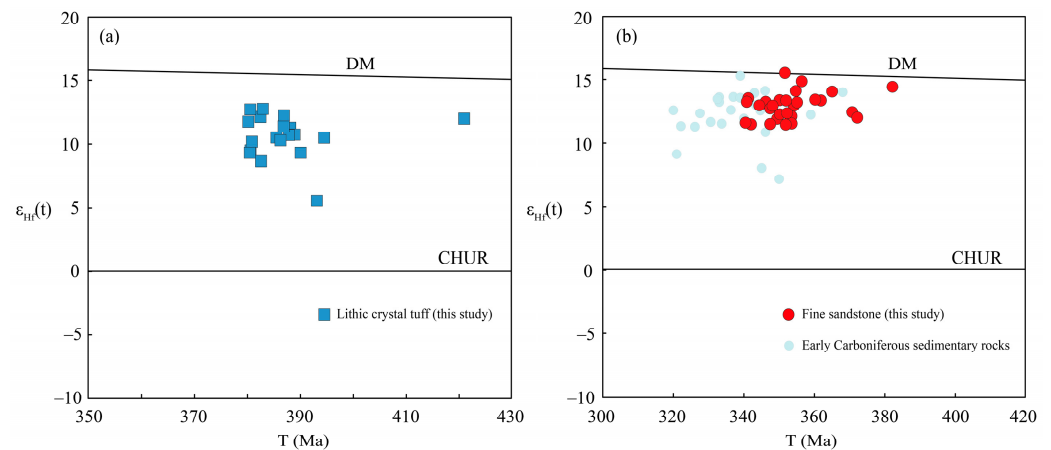


Figure 7. The $\epsilon_{\text{Hf}}(t)$ vs. T (Ma) diagrams of the lithic crystal tuff (a) and fine sandstone (b). Data for the Early Carboniferous sedimentary rocks are from [68].

4.2.1. Major Elements

The lithic crystal tuff samples (19TL-80/81) had high SiO_2 contents (62.32–63.29 wt.%) and medium Na_2O (3.93–4.23 wt.%) and K_2O (1.18–1.36 wt.%) contents. Their MgO contents ranged from 2.38 wt.% to 2.73 wt.%, with a relatively high $\text{Mg}\#$ value of 56. They were plotted in the andesite and dacite fields (Figure 8a) and medium-K calc-alkaline series field (Figure 8b). The $\text{SiO}_2/\text{Al}_2\text{O}_3$ ratios (3.50–3.97) of the fine sandstone samples (19TL-88/89) were comparatively low. These fine sandstone samples had medium $\text{Na}_2\text{O}/\text{K}_2\text{O}$ and relatively high $\text{Fe}_2\text{O}_3/\text{K}_2\text{O}$ ratios, and thus, were plotted in the litharenite fields (Figure 8c).

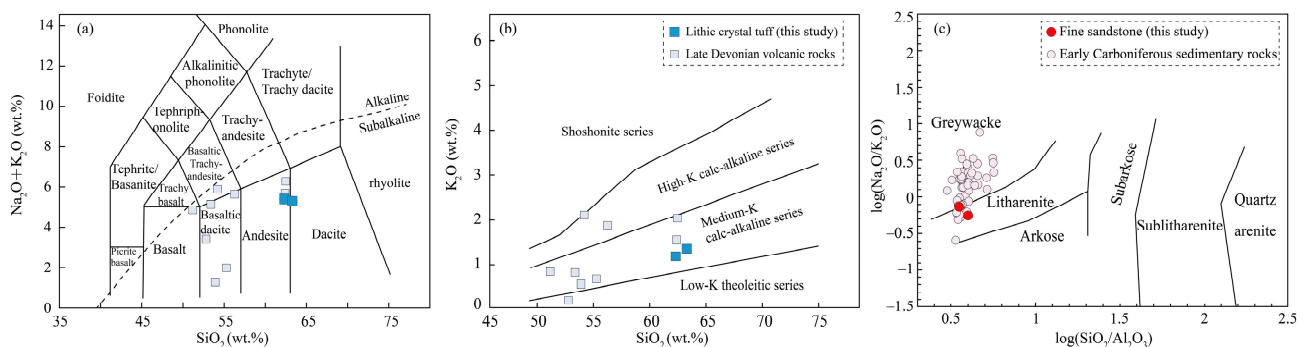


Figure 8. TAS classification diagram ((a), from [69]), SiO_2 vs. K_2O diagram of the lithic crystal tuff ((b), from [70]); $\lg[w(\text{Na}_2\text{O})/(\text{K}_2\text{O})]$ vs. $\lg[w(\text{SiO}_2)/w(\text{Al}_2\text{O}_3)]$ diagram ((c), from [71]) of the fine sandstone. Data for the Late Devonian volcanic rocks and the Early Carboniferous clastic rocks are from [50] and [68,72], respectively.

4.2.2. Trace Elements

The lithic crystal tuff samples showed enrichment of light rare earth elements (LREEs) and depletion of heavy rare earth elements (HREEs) with δEu values of 0.94–0.97 (Figure 9a), implying the absence of obvious Eu anomalies. They were rich in large-ion lithophile elements (LILEs, i.e., Rb, Ba, K) and depleted in high-field-strength elements (HFSEs, i.e., Nb, Ta, Ti), showing similar geochemical characteristics to those of volcanic arc rocks (Figure 9b). The fine sandstone samples had enriched LREEs and relatively flat HREEs (Figure 9c). The δEu values ranged from 0.66 to 0.74, indicating an obvious Eu negative anomaly, similar to that of open PAAS ($\delta\text{Eu} = 0.65$ [73]). The samples were also deficient in HFSEs (i.e., Nb, Ta, Ti) (Figure 9d) and exhibited low ferromagnesian trace element concentrations (Sc, 8.0–8.9; Co, 9.8–11.9; Ni, 4.5–6.5).

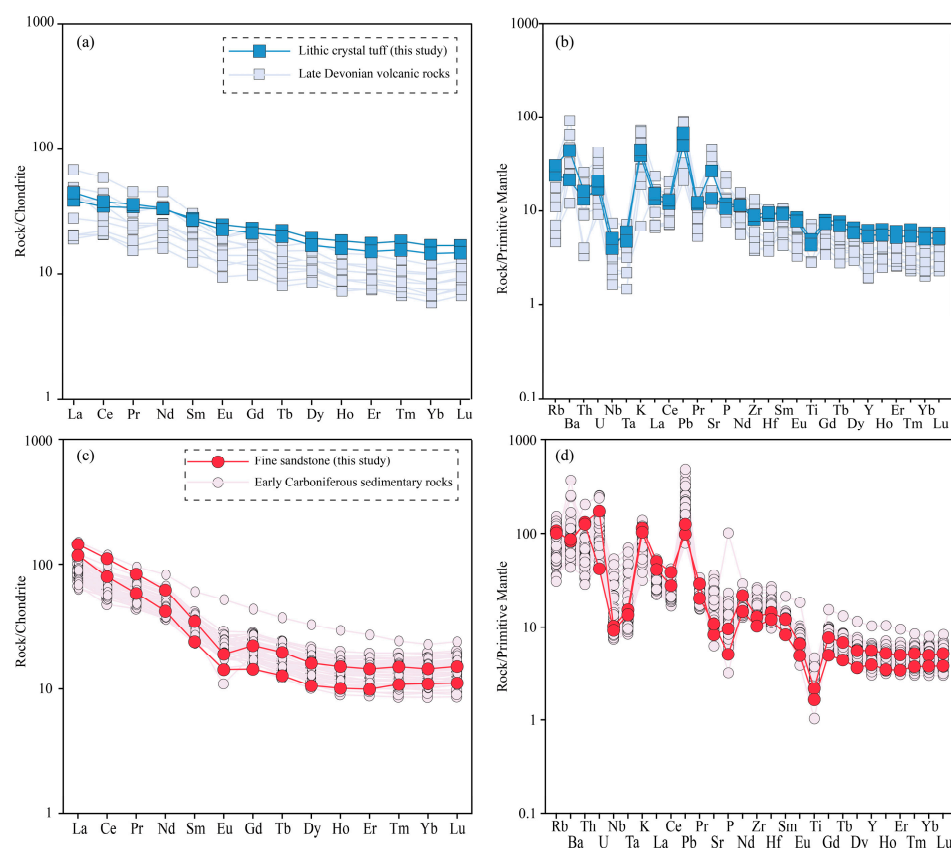


Figure 9. Chondrite-normalized REE patterns (a,c) and primitive-mantle-normalized spidergrams (b,d) of the lithic crystal tuff and fine sandstone. Data for Later Devonian volcanic rocks and Early Carboniferous sedimentary rocks are from [50] and [68,72], respectively.

5. Discussion

5.1. Sedimentary Age of the Kulumudi Formation

Previous work on the stratigraphy of the Middle Devonian Kulumudi Formation was mainly based on the lithostratigraphic correlation and paleontological fossils [31,74]. Among these fossils, occurrences of *Barradeophylum* sp., *Pachyfavosites* sp., *Paraspirifer* sp., *Psilophyton bella* (*Tchirkoua*) *Aneurophyton* aff. *Germanicak* Etw., etc., indicate typical Middle Devonian characteristics [31,74]. In this study, the zircon U-Pb dating result for the lithic crystal tuff from the Middle Devonian Kulumudi Formation was 386 ± 2 Ma (Figure 6b), indicating that the stratum northeast of the Alemale Mountains belongs to the Middle Devonian, which is consistent with previous results [31,74].

Differently, based on the detrital zircon ages, the maximum depositional age of detrital zircons from the fine sandstone was 341 ± 3 Ma (Figure 6c). This result shows that the stratum originally assigned as the “Kulumudi Formation” southwest of the Huojierte Mongolian Township was formed during the Early Carboniferous. Indeed, the result is similar to the age of the adjacent Lower Carboniferous Jiangbasitao Formation (336 ± 3 Ma, 339 ± 2 Ma [51]). Importantly, the originally assigned “Kulumudi Formation” and the Lower Carboniferous Jiangbasitao Formation were invaded by the Late Carboniferous intrusive rocks (318 ± 3 Ma [22]) together (Figure 2). The Jiangbasitao Formation is a set of terrigenous sedimentary rocks mainly composed of the conglomerate, sandy conglomerate, carbonaceous shale, argillaceous siltstone and fine sandstone [31], which is consistent with the rocks observed southwest of the Huojierte Mongolian Township. Thus, our new chronological data, together with the above lithologic correlation, indicate that parts of the “Kulumudi Formation” should be redefined as the Lower Carboniferous Jiangbasitao Formation.

5.2. Tectonic Setting

5.2.1. The Middle Devonian Kulumudi Formation

The lithic crystal tuff samples (~386 Ma) of the Middle Devonian Kulumudi Formation were plotted in the andesite and dacite fields in the TAS classification diagram (Figure 8a), and thus, they belonged to the medium potassium calc-alkaline series (Figure 8b). These samples were rich in LREEs and LILEs and depleted in HREEs and HFSEs (Figure 9a,b), indicating geochemical characteristics similar to the volcanic arc rocks [75]. Furthermore, the samples had relatively low Nb/La ratios (0.32–0.34) and high La/Ta (35.53–53.82) and Th/Nb ratios (0.38–0.39), confirming that they were formed in a subduction-related setting [76]. Their high Ba/La values (16.47–29.58) also imply a strong effect on the magma source area from a subduction zone or related fluids [77]. Furthermore, the $\epsilon_{\text{Hf}}(t)$ values of the zircons from the lithic crystal tuff show highly positive characteristics, ranging from +5.6 to +12.8 (Figure 7a), indicating the feature of a juvenile arc. Considering the whole-rock geochemistry and Hf isotope analysis, the lithic crystal tuff from the Middle Devonian Kulumudi Formation is suggested to be formed in a juvenile arc setting.

5.2.2. The Early Carboniferous Jiangbasitao Formation

The chemical index of alteration (CIA) and index of compositional variability (ICV) can be used to assess the weathering intensity and source composition of the sedimentary rocks. The relatively low CIA values (63.06–63.97) for the fine sandstone from the Jiangbasitao Formation suggest a low degree of chemical weathering. The high ICV values ranging from 1.40–1.45 indicate an immature source. Their δEu values ranged from 0.66 to 0.74 and clear Nb-Ta negative anomalies (Figure 9d), similar to many subduction-related compositionally intermediate lavas [75]. The contents and ratios of major and trace elements in clastic rocks can distinguish different tectonic settings, such as oceanic arc, continental arc, active continental margin and passive continental margin [78,79]. The contents of TiO_2 (0.38–0.50 wt.%) in fine sandstone samples from the Jiangbasitao Formation were similar to those in active continental margin and continental arc [80]. The $\text{Al}_2\text{O}_3/\text{SiO}_2$ (0.25–0.29) and $\text{K}_2\text{O}/\text{Na}_2\text{O}$ (1.29–1.72) ratios were close to those derived from the continental arc and active continental margin, respectively [80]. Moreover, all samples were plotted in the continental arc field in the La-Th-Sc and Th-Sc-Zr/10 tectonic discrimination diagrams (Figure 10a,b). The highly positive $\epsilon_{\text{Hf}}(t)$ values (+11.4 to +15.5) of the detrital zircons from the fine sandstone suggest a juvenile arc (Figure 7b), which is consistent with the interpretation that the Early Carboniferous sedimentary rocks from the Darbut area were derived from a juvenile arc setting (Figure 7b). Thus, combined with published data from adjacent areas [68,72]), the new whole-rock geochemistry and Hf isotope analysis suggest an Early Carboniferous juvenile arc in the central WJT rather than a continental arc with Precambrian basement [13].

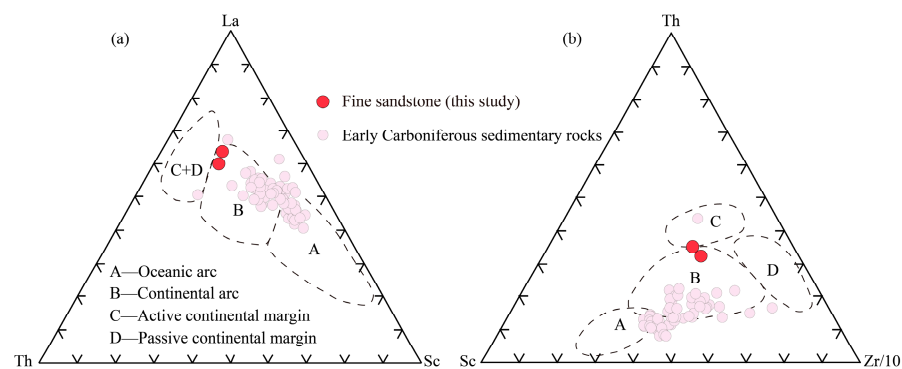


Figure 10. Discrimination diagrams of the La-Th-Sc (a) and Th-Sc-Zr/10 (b) (from [80]). A—oceanic arc; B—continental arc; C—active continental margin; D—passive continental margin. Data for Early Carboniferous sedimentary rocks are from [68,72].

5.3. Tectonic Evolution of West Junggar during the Middle Devonian–Early Carboniferous

During the Ediacaran–Cambrian period, the southern WJT was suggested to be a southward intra-oceanic subduction setting in the Tangbale area, forming the Tangbale ophiolitic mélangé (572–531 Ma [15,20,59–61]). With the northward migration of the subduction zone, the Mayile ophiolite mélangé (516–517 Ma [20,81]) and Barleik ophiolite mélangé (512 ± 7 Ma [81]) gradually formed. These Ediacaran–Early Paleozoic SSZ-type ophiolitic mélangés, combined with the intra-oceanic arc igneous rocks [23] and subduction-related metamorphic rocks [17], clearly indicate an intra-oceanic arc setting for the southern WJT [15]. Meanwhile, the northward subduction of the oceanic crust of the Junggar–Balkhash Ocean formed the Middle Silurian to Early Devonian Boshchekul–Chingiz arc [41].

There are different interpretations of the ocean basin represented by the Darbut–Karamay ophiolite mélangés during the Devonian and Early Carboniferous. Some researchers interpret the basin as a residual ocean basin trapped by the Junggar–Balkhash Ocean under the constraint of the Kazakhstan Orocline [46], based on the fact that the Lower Carboniferous continuous volcano–sedimentary strata are developed on both sides of the Darbut ophiolite mélangé [45,82]. Alternatively, the opening of the Devonian Karamay back-arc ocean basin [41] was suggested to result from the continuous lithosphere extension during the Early–Middle Devonian. Regardless of the residual ocean basin or back-arc ocean basin model, a consensus has been reached about the existence of an Early Devonian–Early Carboniferous oceanic basin in the central WJT. Importantly, previous studies found that the Middle Devonian Kulumudi Formation unconformably overlies the Ediacaran–Early Paleozoic accretionary complexes in the southern and central WJT [20,49,83], indicating that the Ediacaran–Early Paleozoic intra-oceanic subduction had ended before the Middle Devonian [15]. Such a pre-Middle Devonian lateral accretion of juvenile oceanic arc crust was further evidenced by recent dating results of detrital zircons from the southern WJT [12]. A major sedimentary transition from Middle–Late Silurian bathyal facies to Devonian overall littoral–terrestrial facies [49] and the absence of Late Silurian arc-related volcanism also support a pre-Late Silurian termination of the intra-oceanic subduction–accretion processes.

Since the Early Devonian, the oceanic crust represented by the Darbut–Karamay ophiolitic mélangés has subducted southward, forming the active continental margin in the southern and central WJT. Early–Middle Devonian adakitic magmatism (394–390 Ma) with high positive $\varepsilon_{\text{Hf}}(t)$ values of +5.6 to +10.3 was newly recognized in the southern WJT and their formation was contributed to the partial melting of a juvenile and slightly thickened lower crust as the eastern extension of the Kazakhstan Early–Middle Devonian OAB [10]. Similarly, Liu and Han [9] suggested that the tectonic setting of the central WJT (northern IAB) evolved to a juvenile Late Devonian IAB built on Ediacaran–Early Paleozoic accreted terranes (intra-oceanic arcs and accretionary complexes), contrasting with the Yili (southern IAB) and Balkhash (central IAB) arcs built on a Precambrian continental basement. Combined with the above-published results, the positive $\varepsilon_{\text{Hf}}(t)$ values of the studied Middle Devonian tuff (+5.6–+12.8) and Early Carboniferous sandstone (+11.4–+15.5) show typical juvenile arc characteristics, indicating that the active continental margin of central WJT lacked ancient continental basement during the Middle Devonian–Early Carboniferous subduction [9,10]. The occurrences of only two ancient zircons for pyroxene diorite (408 Ma [13]) from the central WJT may not indicate a Precambrian basement. Thus, it was concluded that the southward subduction of the ocean basin represented by the Darbut–Karamay ophiolitic mélangés beneath the newly accreted arc crustal segments resulted in a juvenile arc with positive Hf isotope characteristics.

6. Conclusions

- (1) The lithic crystal tuff from the Kulumudi Formation northeast of the Alemale Mountains in the Laofengkou area yielded a zircon U–Pb age of 386 ± 2 Ma and was formed during the Middle Devonian. The maximum depositional age for the fine sandstone originally assigned into the “Kulumudi Formation” southwest of the Huo-

jierte Mongolian Township was 341 ± 3 Ma, belonging to the Lower Carboniferous Jiangbasitao Formation.

- (2) According to the whole-rock geochemistry and Hf isotope analysis, the Middle Devonian Kulumudi Formation and Lower Carboniferous Jiangbasitao Formation formed in a juvenile arc setting related to the ocean–continent subduction.
- (3) During the Middle Devonian to Early Carboniferous, the ocean basin represented by the Darbut–Karamay ophiolitic mélanges subducted southward beneath the newly accreted arc crustal segments, forming a juvenile arc with positive Hf isotopic characteristics.

Supplementary Materials: The following supporting information can be downloaded at: <https://www.mdpi.com/article/10.3390/min14010014/s1>, Table S1: Zircon U-Pb data of pyroclastic rocks and sedimentary rocks from the Laofengkou area, West Junggar; Table S2: Rare earth element compositions ($\times 10^{-6}$) of zircons for pyroclastic rocks and sedimentary rocks from the Laofengkou area, West Junggar; Table S3: Zircon in situ Lu-Hf isotope compositions for pyroclastic rocks and sedimentary rocks from the Laofengkou area, West Junggar; Table S4: Whole-rock major (wt.%) and trace element ($\times 10^{-6}$) compositions for pyroclastic rocks and sedimentary rocks from the Laofengkou area, West Junggar.

Author Contributions: Conceptualization, B.L.; methodology, B.L.; software, L.-X.H. and Z.-H.X.; formal analysis, L.-X.H. and J.-X.M.; investigation, Y.-B.-H.H.; writing—original draft preparation, B.L. and L.-X.H.; writing—review and editing, B.L. and Y.X.; funding acquisition, N.J. All authors have read and agreed to the published version of the manuscript.

Funding: This study was supported by the National Key R&D Program of China (2023YFB2603602); National Natural Science Foundation of China (41802236, 42102087, U2244201); China Postdoctoral Science Foundation (2022M712966); Second Tibetan Plateau Scientific Expedition and Research (2021QZKK0304); “the Fundamental Research Funds for the Central Universities” (N2201014); “the Fundamental Research Funds for the Educational Department of Liaoning Province” (JYTMS20230617); and Opening Foundation of State Key Laboratory of Continental Dynamics, Northwest University (20LCD07).

Data Availability Statement: The authors confirm that all data are presented in the paper.

Acknowledgments: Three anonymous reviewers are thanked for their constructive comments. We are particularly grateful to Zhi-An Bao for help with the zircon Hf isotopic analyses at Northwest University. We thank Jia-Wei Li and Chen He for their help in the field.

Conflicts of Interest: The authors declare no conflict of interest.

References

1. Şengör, A.M.C.; Natal'in, B.A.; Burtman, V.S. Evolution of the Altaid tectonic collage and Palaeozoic crustal growth in Eurasia. *Nature* **1993**, *364*, 299–307. [[CrossRef](#)]
2. Windley, B.F.; Alexeiev, D.; Xiao, W.J.; Kröner, A.; Badarch, G. Tectonic models for accretion of the Central Asian Orogenic Belt. *J. Geol. Soc.* **2007**, *164*, 31–47. [[CrossRef](#)]
3. Kröner, A.; Hegner, E.; Lehmann, B.; Heinhorst, J.; Wingate, M.T.D.; Liu, D.Y.; Ermelov, P. Palaeozoic arc magmatism in the Central Asian Orogenic Belt of Kazakhstan: SHRIMP zircon ages and whole-rock Nd isotopic systematics. *J. Asian Earth Sci.* **2008**, *32*, 118–130. [[CrossRef](#)]
4. Li, P.; Sun, M.; Rosenbaum, G.; Yuan, C.; Safonova, I.; Cai, K.; Jiang, Y.; Zhang, Y. Geometry, kinematics and tectonic models of the Kazakhstan Orocline, Central Asian Orogenic Belt. *J. Asian Earth Sci.* **2018**, *153*, 42–56. [[CrossRef](#)]
5. Xiao, W.; Windley, B.F.; Sun, S.; Li, J.; Huang, B.; Han, C.; Yuan, C.; Sun, M.; Chen, H. A Tale of Amalgamation of Three Permo-Triassic Collage Systems in Central Asia: Oroclines, Sutures, and Terminal Accretion. *Annu. Rev. Earth Planet. Sci.* **2015**, *43*, 477–507. [[CrossRef](#)]
6. Liu, Y.; Xiao, W.; Ma, Y.; Li, S.; Peskov, A.Y.; Chen, Z.; Zhou, T.; Guan, Q. Oroclines in the Central Asian Orogenic Belt. *Natl. Sci. Rev.* **2023**, *10*, nwac243. [[CrossRef](#)]
7. Xiao, W.; Han, C.; Yuan, C.; Sun, M.; Lin, S.; Chen, H.; Li, Z.; Li, J.; Sun, S. Middle Cambrian to Permian subduction-related accretionary orogenesis of Northern Xinjiang, NW China: Implications for the tectonic evolution of central Asia. *J. Asian Earth Sci.* **2008**, *32*, 102–117. [[CrossRef](#)]

8. Choulet, F.; Cluzel, D.; Faure, M.; Lin, W.; Wang, B.; Chen, Y.; Wu, F.; Ji, W. New constraints on the pre-Permian continental crust growth of Central Asia (West Junggar, China) by U-Pb and Hf isotopic data from detrital zircon: Pre-Permian continental crust growth of Central Asia. *Terra Nova* **2012**, *24*, 189–198. [[CrossRef](#)]
9. Liu, B.; Han, B.F. Identification of lateral inhomogeneity of arc basement by reconstructing the Late Devonian arc belt in the southwestern Central Asian Orogenic Belt. *J. Geodyn.* **2019**, *132*, 101668. [[CrossRef](#)]
10. Ren, R.; Liu, B.; Han, B.F.; Guan, S.W. Early-Middle Devonian adakitic magmatism generated by slab retreat in southern West Junggar, NW China: Implications for tectonic correlation with central and East Kazakhstan. *Int. Geol. Rev.* **2023**, *65*, 2315–2331. [[CrossRef](#)]
11. Safonova, I.; Perfilova, A. Survived and disappeared intra-oceanic arcs of the Paleo-Asian Ocean: Evidence from Kazakhstan. *Natl. Sci. Rev.* **2023**, *10*, nwac215. [[CrossRef](#)] [[PubMed](#)]
12. Zhang, P.; Wang, G.C.; Shen, T.; Polat, A.; Zhu, C. Paleozoic convergence processes in the southwestern Central Asian Orogenic Belt: Insights from U–Pb dating of detrital zircons from West Junggar, northwestern China. *Geosci. Front.* **2021**, *12*, 531–548. [[CrossRef](#)]
13. Wu, C.; Hong, T.; Xu, X.-W.; Cao, M.-J.; Li, H.; Zhang, G.-L.; You, J.; Ke, Q.; Dong, L.-H. Tectonic evolution of the Paleozoic Barluk continental arc, West Junggar, NW China. *J. Asian Earth Sci.* **2018**, *160*, 48–66. [[CrossRef](#)]
14. Han, B.F.; Guo, Z.J.; He, G.Q. Timing of major suture zones in North Xinjiang, China: Constraints from stitching plutons. *Acta Petrol. Sin.* **2010**, *26*, 2233–2246. (In Chinese with English abstract)
15. Liu, B.; Han, B.F.; Xu, Z.; Ren, R.; Chen, J.F. The Ediacaran to Early Paleozoic evolution of the Junggar–Balkhash Ocean: A synthesis of the ophiolitic mélanges in the southern West Junggar terrane, NW China. *Geol. J.* **2020**, *55*, 1689–1707. [[CrossRef](#)]
16. Chen, B.; Arakawa, Y. Elemental and Nd-Sr isotopic geochemistry of granitoids from the West Junggar foldbelt (NW China), with implications for Phanerozoic continental growth. *Geochim. Cosmochim. Acta* **2005**, *69*, 1307–1320. [[CrossRef](#)]
17. Liu, B.; Han, B.-F.; Xu, Z.; Ren, R.; Zhang, J.-R.; Zhou, J.; Su, L.; Li, Q.-L. The Cambrian initiation of intra-oceanic subduction in the southern Paleo-Asian Ocean: Further evidence from the Barleik subduction-related metamorphic complex in the West Junggar region, NW China. *J. Asian Earth Sci.* **2016**, *123*, 1–21. [[CrossRef](#)]
18. Liu, B.; Han, B.F.; Ren, R.; Chen, J.F.; Wang, Z.Z.; Zheng, B. Petrogenesis and tectonic implications of the Early Carboniferous to the Late Permian Barleik plutons in the West Junggar (NW China). *Lithos* **2017**, *272–273*, 232–248. [[CrossRef](#)]
19. Xu, Z.; Han, B.-F.; Ren, R.; Zhou, Y.-Z.; Zhang, L.; Chen, J.-F.; Su, L.; Li, X.-H.; Liu, D.-Y. Ultramafic–mafic mélange, island arc and post-collisional intrusions in the Mayile Mountain, West Junggar, China: Implications for Paleozoic intra-oceanic subduction–accretion process. *Lithos* **2012**, *132–133*, 141–161. [[CrossRef](#)]
20. Ren, R.; Han, B.-F.; Xu, Z.; Zhou, Y.-Z.; Liu, B.; Zhang, L.; Chen, J.-F.; Su, L.; Li, J.; Li, X.-H.; et al. When did the subduction first initiate in the southern Paleo-Asian Ocean: New constraints from a Cambrian intra-oceanic arc system in West Junggar, NW China. *Earth Planet. Sci. Lett.* **2014**, *388*, 222–236. [[CrossRef](#)]
21. Liu, B.; Han, B.F.; Chen, J.F.; Ren, R.; Zheng, B.; Wang, Z.Z.; Feng, L.X. Closure time of the Junggar-Balkhash Ocean: Constraints from Late Paleozoic volcano-sedimentary sequences in the Barleik Mountains, West Junggar, NW China. *Tectonics* **2017**, *36*, 2823–2845. [[CrossRef](#)]
22. Zheng, B.; Han, B.F.; Liu, B.; Wang, Z.Z. Ediacaran to Paleozoic magmatism in West Junggar Orogenic Belt, NW China, and implications for evolution of Central Asian Orogenic Belt. *Lithos* **2019**, *338–339*, 111–127. [[CrossRef](#)]
23. Liao, W.; Han, B.F.; Xu, Y.; Li, A. Ediacaran initial subduction and Cambrian slab rollback of the Junggar Ocean: New evidence from igneous tectonic blocks and gabbro enclave in Early Palaeozoic accretionary complexes, southern West Junggar, NW China. *Geol. Mag.* **2021**, *158*, 1811–1829. [[CrossRef](#)]
24. Chen, J.F.; Han, B.F.; Ji, J.Q.; Zhang, L.; Xu, Z.; He, G.Q.; Wang, T. Zircon U–Pb ages and tectonic implications of Paleozoic plutons in northern West Junggar, North Xinjiang, China. *Lithos* **2010**, *115*, 137–152. [[CrossRef](#)]
25. Gao, R.; Xiao, L.; Pirajno, F.; Wang, G.C.; He, X.X.; Yang, G.; Yan, S.W. Carboniferous–Permian extensive magmatism in the West Junggar, Xinjiang, northwestern China: Its geochemistry, geochronology, and petrogenesis. *Lithos* **2014**, *204*, 125–143. [[CrossRef](#)]
26. Han, B.F.; Ji, J.Q.; Song, B.; Chen, L.H.; Zhang, L. Late Paleozoic vertical growth of continental crust around the Junggar Basin, Xinjiang, China (part I): Timing of postcollisional plutonism. *Acta Petrol. Sin.* **2006**, *22*, 1077–1086. (In Chinese with English abstract)
27. Hong, Y.B.H.; Liu, B.; Han, B.F.; Ma, J.X.; Chen, J.D. Late Carboniferous closure of the Junggar-Balkhash Ocean: Insights from the early Permian post-accretionary magmatism in the Barleik Mountains of West Junggar, NW China. *Lithos* **2022**, *432–433*, 106900. [[CrossRef](#)]
28. Geng, H.; Sun, M.; Yuan, C.; Xiao, W.; Xian, W.; Zhao, G.; Zhang, L.; Wong, K.; Wu, F. Geochemical, Sr–Nd and zircon U–Pb–Hf isotopic studies of Late Carboniferous magmatism in the West Junggar, Xinjiang: Implications for ridge subduction? *Chem. Geol.* **2009**, *266*, 364–389. [[CrossRef](#)]
29. Tang, G.J.; Wang, Q.; Wyman, D.A.; Li, Z.X.; Zhao, Z.H.; Jia, X.H.; Jiang, Z.Q. Ridge subduction and crustal growth in the Central Asian Orogenic Belt: Evidence from Late Carboniferous adakites and high-Mg diorites in the western Junggar region, northern Xinjiang (west China). *Chem. Geol.* **2010**, *277*, 281–300. [[CrossRef](#)]
30. Zhang, J.E.; Chen, Y.C.; Xiao, W.J.; Wakabayashi, J.; Windley, B.F.; Yin, J. Sub-parallel ridge-trench interaction and an alternative model for the Silurian-Devonian archipelago in Western Junggar and North-Central Tianshan in NW China. *Earth-Sci. Rev.* **2021**, *217*, 103648. [[CrossRef](#)]

31. XBGMR (Xinjiang Bureau of Geology and Mineral Resources, Xinjiang, China). *Regional Geological Map of Tuoli Area (L-44-XXIV)*; Map Scale 1:200 000; XBGMR: Urumqi, China, 1975. (In Chinese)
32. Wang, J.R.; Jia, Z.L.; Li, T.D.; Ma, J.L.; Zhao, L.; He, Y.B.; Zhang, W.; Liu, K.X. Discovery of Early Devonian adakite in West Junggar, Xinjiang: Implications for geotectonics and Cu mineralization. *Acta Petrol. Sin.* **2013**, *29*, 840–852. (In Chinese with English abstract)
33. Han, B.F.; He, G.Q.; Wang, S.G. Postcollisional mantle-derived magmatism, underplating and implications for basement of the Junggar Basin. *Sci. China Ser. D Earth Sci.* **1999**, *42*, 113–119. [[CrossRef](#)]
34. Zheng, B.; Han, B.F.; Wang, Z.Z.; Liu, B.; Feng, L.X. An example of Phanerozoic continental crustal growth: The West Junggar Orogenic Belt, Northwest China. *Lithos* **2020**, *376*, 105745. [[CrossRef](#)]
35. Zhao, L.; He, G.Q. Geochronology and geochemistry of the Cambrian (~518 Ma) Chagantaolegai ophiolite in northern West Junggar (NW China): Constraints on spatiotemporal characteristics of the Chingiz–Tarbagatai megazone. *Int. Geol. Rev.* **2014**, *56*, 1181–1196. [[CrossRef](#)]
36. Yang, Y.Q.; Zhao, L.; Zheng, R.G.; Xu, Q.Q. Evolution of the early Paleozoic Hongguleleng–Balkybye Ocean: Evidence from the Hebuke-saier ophiolitic mélange in the northern West Junggar, NW China. *Lithos* **2019**, *324–325*, 519–536. [[CrossRef](#)]
37. Xu, Z.; Han, B.F.; Ren, R.; Zhou, Y.Z.; Su, L. Palaeozoic multiphase magmatism at Barleik Mountain, southern West Junggar, Northwest China: Implications for tectonic evolution of the West Junggar. *Int. Geol. Rev.* **2013**, *55*, 633–656. [[CrossRef](#)]
38. Yang, Y.Q.; Zhao, L.; Zhang, J.; Niu, M.L. Middle Paleozoic archipelago amalgamation and tectonic transform in the northern West Junggar, NW China: Constraints from magmatism and deformation. *Gondwana Res.* **2021**, *98*, 147–165. [[CrossRef](#)]
39. Yin, J.; Chen, W.; Yuan, C.; Yu, S.; Xiao, W.; Long, X.; Li, J.; Sun, J. Petrogenesis of Early Carboniferous adakitic dikes, Sawur region, northern West Junggar, NW China: Implications for geodynamic evolution. *Gondwana Res.* **2015**, *27*, 1630–1645. [[CrossRef](#)]
40. Xu, Y.; Han, B.F.; Liao, W.; Li, A. The Serpukhovian–Bashkirian Amalgamation of Laurussia and the Siberian Continent and Implications for Assembly of Pangea. *Tectonics* **2022**, *41*, e2022TC007218. [[CrossRef](#)]
41. Chen, J.F.; Han, B.F.; Zhang, L.; Xu, Z.; Liu, J.L.; Qu, W.J.; Li, C.; Yang, J.H.; Yang, Y.H. Middle Paleozoic initial amalgamation and crustal growth in the West Junggar (NW China): Constraints from geochronology, geochemistry and Sr–Nd–Hf–Os isotopes of calc-alkaline and alkaline intrusions in the Xiemisitai–Saier Mountains. *J. Asian Earth Sci.* **2015**, *113*, 90–109. [[CrossRef](#)]
42. Shen, P.; Shen, Y.C.; Li, X.H.; Pan, H.D.; Zhu, H.P.; Meng, L.; Dai, H.W. Northwestern Junggar Basin, Xiemisitai Mountains, China: A geochemical and geochronological approach. *Lithos* **2012**, *140–141*, 103–118. [[CrossRef](#)]
43. Yin, J.Y.; Chen, W.; Xiao, W.J.; Yuan, C.; Windley, B.F.; Yu, S.; Cai, K.D. Late Silurian–early Devonian adakitic granodiorite, A-type and I-type granites in NW Junggar, NW China: Partial melting of mafic lower crust and implications for slab roll-back. *Gondwana Res.* **2017**, *43*, 55–73. [[CrossRef](#)]
44. Gu, P.Y.; Li, Y.J.; Zhang, B.; Tong, L.L.; Wang, J.N. LA-ICP-MS zircon U–Pb dating of gabbro in the Darbut ophiolite, western Junggar, China. *Acta Petrol. Silica* **2009**, *25*, 1364–1372. (In Chinese with English abstract)
45. Chen, S.; Guo, Z.J. Time constraints, tectonic setting of Dalabute ophiolitic complex and its significance for Late Paleozoic tectonic evolution in West Junggar. *Acta Petrol. Sin.* **2010**, *26*, 2336–2344. (In Chinese with English abstract)
46. Chen, S.; Pe-Piper, G.; Piper, D.J.W.; Guo, Z. Ophiolitic mélanges in crustal-scale fault zones: Implications for the Late Palaeozoic tectonic evolution in West Junggar, China: Fault-zone ophiolite, West Junggar. *Tectonics* **2014**, *33*, 2419–2443. [[CrossRef](#)]
47. Zhao, L.; He, G.Q. LA-ICP-MS zircon age of dacite in Tailegula Formation and their constraints on emplacement of darbut ophiolite in West Junggar. *Acta Sci. Nat. Univ. Pekin.* **2016**, *52*, 871–880. (In Chinese with English abstract)
48. Bai, J.K.; Chen, J.L.; Tang, Z.; Zhang, Y. Redefinition of the Middle Devonian Kulumudi Formation in the south of Tiechangou town, West Junggar, Xinjiang and its geological implications. *Northwestern Geol.* **2015**, *48*, 72–80. (In Chinese with English abstract)
49. Bai, J.K.; Chen, J.L.; Yan, Z.; Tang, Z.; Xu, X.Y.; Li, J.L. The timing of opening and closure of the Mayile oceanic basin: Evidence from the angular unconformity between the Middle Devonian and its underlying geological body in the southern West Junggar. *Acta Petrol. Sin.* **2015**, *31*, 133–142. (In Chinese with English abstract)
50. Xiang, K.P.; Li, Y.J.; Li, Z.; Wang, R.; Yang, G.X.; Duan, F.H.; Li, G.Y. LA ICP-MS zircon age and geochemistry of the Aladeyikesai Formation volcanic rocks in the Halaalate Mountain of West Junggar, Xinjiang, and their tectonic significance. *Acta Geol. Sin.* **2015**, *89*, 843–855. (In Chinese with English abstract) [[CrossRef](#)]
51. Fan, T.T.; Zhou, X.H.; Liu, Y.Q.; Li, W.; Zheng, Z.Y.; Hu, T.; Liang, H. Crystal Tuff Zircon LA-ICP-MS U–Pb Ages from the Lower Jiangbasitao Formation in the East Daheishan Area Xinjiang and Their Geological Implications. *Acta Sedimentol. Sin.* **2011**, *29*, 312–320. (In Chinese with English abstract)
52. Guo, L.S.; Liu, Y.L.; Wang, Z.H.; Song, D.; Xu, F.J.; Su, L. The zircon U–Pb LA-ICP-MS geochronology of volcanic rocks in Baogutu areas, western Junggar. *Acta Petrol. Sin.* **2010**, *26*, 471–477. (In Chinese with English abstract)
53. Li, Y.J.; Tong, L.L.; Zhang, B.; Liu, J.; Zhang, T.J.; Wang, J.N. On the old and new relationship between Xibeikulasi formation and Baogutu formation of the Carboniferous system, West Junggar. *Xinjiang Geol.* **2010**, *28*, 130–136. (In Chinese with English abstract)
54. Gong, Y.M.; Zong, R.W. Paleozoic Stratigraphic Regionalization and Paleogeographic Evolution in Western Junggar, Northwestern China. *Earth Sci.-J. China Univ. Geosci.* **2015**, *40*, 461–484. (In Chinese with English abstract)
55. An, F.; Wei, S.N.; Fang, Z.K.; Zheng, B.; Deng, Y. Petrology and zircon U–Pb geochronology of tuffaceous conglomerate in the Xibeikulasi Formation, West Junggar, and its implication for sedimentary sequence. *Acta Geol. Sin.* **2019**, *93*, 1954–1967. (In Chinese with English abstract)

56. Dou, Y.W.; Sun, Z.H. The Age of Harjiawu Formation and Karagang Formation in North Xinjiang. *Geol. Rev.* **1985**, *31*, 489–494. (In Chinese with English abstract)
57. Li, J.W.; Liu, B.; Han, B.F.; Hong, Y.B.H. Identification of a Late Carboniferous Angular Unconformity in the Jiayier Mountains of the West Junggar and its Constraints on the Closure Time of the Junggar-Balkhash Ocean. *Geotecton. Metallog.* **2023**, *47*, 284–307. (In Chinese with English abstract) [[CrossRef](#)]
58. Wen, Z.G.; Wang, H.Q.; Du, Y.; Liu, S.B.; Wang, J.W. The formation age and tectonic significance of Yemuqi granite in WestJunggar, Xinjiang. *Geol. Bull. China* **2019**, *38*, 1297–1305. (In Chinese with English abstract)
59. Kwon, S.T.; Tilton, G.R.; Coleman, R.G.; Feng, Y. Isotopic studies bearing on the tectonics of the West Junggar Region, Xinjiang, China. *Tectonics* **1989**, *8*, 719–727. [[CrossRef](#)]
60. Jian, P.; Liu, D.Y.; Shi, Y.R.; Zhang, F.Q. SHRIMP dating of SSZ ophiolites from Northern Xinjiang Province, China: Implications for generation of oceanic crust in the central Asian orogenic belt. In *Structural and Tectonic Correlation across the Central Asia Orogenic Collage: North-Eastern Segment. Guidebook and Abstract Volume of the Siberian Workshop IGCP-480*; Sklyarov, E.V., Ed.; IEC SB RAS: Irkutsk, Russia, 2005; Volume 246.
61. Yang, G.; Li, Y.; Santosh, M.; Gu, P.; Yang, B.; Zhang, B.; Wang, H.; Zhong, X.; Tong, L. A Neoproterozoic seamount in the Paleasian Ocean: Evidence from zircon U–Pb geochronology and geochemistry of the Mayile ophiolitic mélange in West Junggar, NW China. *Lithos* **2012**, *140–141*, 53–65. [[CrossRef](#)]
62. Liu, Y.S.; Hu, Z.C.; Gao, S.; Günther, D.; Xu, J.; Gao, C.G.; Chen, H.H. In situ analysis of major and trace elements of anhydrous minerals by LA-ICP-MS without applying an internal standard. *Chem. Geol.* **2008**, *257*, 34–43. [[CrossRef](#)]
63. Yuan, H.L.; Gao, S.; Dai, M.N.; Zong, C.L.; Günther, D.; Fontaine, G.H.; Liu, X.M.; Diwu, C.R. Simultaneous determinations of U–Pb age, Hf isotopes and trace element compositions of zircon by excimer laser-ablation quadrupole and multiple-collector ICP-MS. *Chem. Geol.* **2008**, *247*, 100–118. [[CrossRef](#)]
64. Bao, Z.A.; Chen, K.Y.; Kang, L.; Zong, C.L.; Nie, X.J.; Lv, N.; Liang, P.; Yuan, H.L. Comparison of synthetic zircon, high-temperature and high-pressure sintered zircon and fast hot-pressing sintered zircon for in situ hafnium isotope analysis by LA-MC-ICP-MS. *J. Anal. At. Spectrom.* **2023**, *38*, 2313–2323. [[CrossRef](#)]
65. Lan, Z.W.; Huyskens, M.H.; Le Hir, G.; Mitchell, R.N.; Yin, Q.Z.; Zhang, G.Y.; Li, X.H. Massive volcanism may have foreshortened the Marinoan snowball Earth. *Geophys. Res. Lett.* **2022**, *49*, e2021GL097156. [[CrossRef](#)]
66. Hoskin, P.W.O. Trace-element composition of hydrothermal zircon and the alteration of Hadean zircon from the Jack Hills, Australia. *Geochim. Cosmochim. Acta* **2005**, *69*, 637–648. [[CrossRef](#)]
67. Sun, S.S.; McDonough, W.F. Chemical and isotopic systematics of oceanic basalts: Implications for mantle composition and processes. *Geol. Soc. Lond. Spec. Publ.* **1989**, *42*, 313–345. [[CrossRef](#)]
68. Weng, K.; Dong, Y.P.; Xu, X.Y.; Ma, Z.P.; Chen, B. Carboniferous sedimentary provenance and tectonic setting in the Darbut region of Western Junggar (NW China): Evidence from mineralogy, geochemistry and detrital zircon U–Pb dating. *J. Geol. Soc.* **2021**, *178*, jgs2020-132. [[CrossRef](#)]
69. Le Bas, M.J.; Le Maitre, R.W.; Streckeisen, A.; Zanettin, B. A Chemical Classification of Volcanic Rocks Based on the Total Alkali-Silica Diagram. *J. Petrol.* **1986**, *27*, 745–750. [[CrossRef](#)]
70. Peccerillo, A.; Taylor, S.R. Geochemistry of eocene calc-alkaline volcanic rocks from the Kastamonu area, Northern Turkey. *Contrib. Mineral. Petrol.* **1976**, *58*, 63–81. [[CrossRef](#)]
71. Pettijohn, F.J.; Potter, P.E.; Siever, R. *Sand and Sandstone*; Springer: Berlin/Heidelberg, Germany, 1972. [[CrossRef](#)]
72. Tao, H.F.; Sun, S.; Wang, Q.C.; Yang, X.F.; Jiang, L. Petrography and geochemistry of lower carboniferous greywacke and mudstones in Northeast Junggar, China: Implications for provenance, source weathering, and tectonic setting. *J. Asian Earth Sci.* **2014**, *87*, 11–25. [[CrossRef](#)]
73. Taylor, S.T.; McLennan, S.M. *The Continental Crust: Composition and Evolution*; Blackwell: Oxford, UK, 1985; Volume 312.
74. Wei, R.Z.; Dong, A.G.; Li, S.; Wang, R.J.; Chai, J.Z. Discovery and significance of Early Devonian fossils in the Mayileshan area, western Junggar, Xinjiang, China. *Geol. Bull. China* **2011**, *30*, 101–105. (In Chinese with English abstract)
75. Stolz, A.J.; Jochum, K.P.; Spettel, B.; Hofmann, A.W. Fluid- and melt-related enrichment in the subarc mantle: Evidence from Nb/Ta variations in island-arc basalts. *Geology* **1996**, *24*, 587–590. [[CrossRef](#)]
76. Condie, K.C. Geochemistry and Tectonic Setting of Early Proterozoic Supracrustal Rocks in the Southwestern United States. *J. Geol.* **1986**, *94*, 845–864. [[CrossRef](#)]
77. Edwards CM, H.; Morris, J.D.; Thirlwall, M.F. Separating mantle from slab signatures in arc lavas using B/Be and radiogenic isotope systematics. *Nature* **1993**, *362*, 530–533. [[CrossRef](#)]
78. Bhatia, M.R. Plate Tectonics and Geochemical Composition of Sandstones: A Reply. *J. Geol.* **1985**, *93*, 85–87. [[CrossRef](#)]
79. Bhatia, M.R.; Crook, K.A.W. Trace element characteristics of graywackes and tectonic setting discrimination of sedimentary basins. *Contrib. Mineral. Petrol.* **1986**, *92*, 181–193. [[CrossRef](#)]
80. Bhatia, M.R. Plate Tectonics and Geochemical Composition of Sandstones. *J. Geol.* **1983**, *91*, 611–627. [[CrossRef](#)]
81. Zhao, W.P. Paleozoic stratigraphic division in the south of western Junggar and some problems about Barleik ophiolites. In *Proceedings of the International Workshop on the Large Balkash–Western Junggar Copper–Gold Province, Karamay, China, 22–27 August 2011*; pp. 32–39. (In Chinese with English abstract)

82. Chen, S.; Guo, Z.J.; Pe-Piper, G.; Zhu, B.B. Late Paleozoic peperites in West Junggar, China, and how they constrain regional tectonic and palaeoenvironmental setting. *Gondwana Res.* **2013**, *23*, 666–681. [[CrossRef](#)]
83. Zhang, J.E.; Xiao, W.J.; Luo, J.; Chen, Y.C.; Windley, B.F.; Song, D.F.; Han, C.M.; Safonova, I. Collision of the Tacheng block with the Mayile-Barleik-Tangbale accretionary complex in Western Junggar, NW China: Implication for Early-Middle Paleozoic architecture of the western Altai. *J. Asian Earth Sci.* **2018**, *159*, 259–278. [[CrossRef](#)]

Disclaimer/Publisher’s Note: The statements, opinions and data contained in all publications are solely those of the individual author(s) and contributor(s) and not of MDPI and/or the editor(s). MDPI and/or the editor(s) disclaim responsibility for any injury to people or property resulting from any ideas, methods, instructions or products referred to in the content.